Visible Light Absorption of Binuclear $TiOCo^{II}$ Charge-Transfer Unit Assembled in Mesoporous Silica

Hongxian Han and Heinz Frei*

Physical Biosciences Division, Lawrence Berkeley National Laboratory, University of California, Berkeley, CA 9720

Abstract

Grafting of $Co^{II}(NCCH_3)_2Cl_2$ onto mesoporous Ti-MCM-41 silica in acetonitrile solution affords binuclear Ti-O-Co^{II} sites on the pore surface under complete replacement of the precursor ligands by interactions with anchored Ti centers and the silica surface. The Co^{II} ligand field spectrum signals that the Co centers are anchored on the pore surface in tetrahedral coordination. FT-infrared action spectroscopy using ammonia gas adsorption reveals Co-O-Si bond modes at 831 and 762 cm^{-1}. No Co oxide clusters are observed in the as-synthesized material. The bimetallic moieties feature an absorption extending from the UV into the visible to about 600 nm which is attributed to the Ti^{IV}-O-Co^{II} → Ti^{III}-O-Co^{III} metal-to-metal charge-transfer (MMCT) transition. The chromophore is absent in MCM-41 containing Ti and Co centers isolated from each other; this material was synthesized by grafting Co^{II} onto a Ti-MCM-41 sample with the Ti centers protected by a cyclopentadienyl ligand. The result indicates that the appearance of the charge-transfer absorption requires that the metal centers are linked by an oxo bridge, which is additionally supported by XANES spectroscopy. The MMCT chromophore of Ti-O-Co^{II} units has sufficient oxidation power to serve as visible light electron pump for driving multi-electron transfer catalysts of demanding uphill reactions such as water oxidation.

1. Introduction

Robust, inert mesoporous solids such as silica offer opportunities for arranging and coupling polynuclear metal oxide units for photosynthetic transformations such as carbon dioxide reduction and water oxidation. The pore surface chemistry of silanol-rich silica materials like MCM-41 is suitable for assembling and covalent anchoring of polynuclear moieties. Equally importantly, the very high surface area of the support allows to accommodate photocatalytic sites at sufficient density so that catalytic rates are able to keep up with the solar flux, and nanostructured features of the support offer ways to separate catalytic reduction from oxidation sites. We have recently assembled binuclear units of type Ti-O-Cu^{I}, Ti-O-Sn^{II}, Zr-O-Cu^{I} in the 30 A pores of MCM-41.[1,2] These units are covalently anchored on the silica pore surface and possess a metal-to-metal charge-transfer (MMCT) absorption with a tail extending into the visible spectral region. In the case of the material with anchored Zr-O-Cu^{I} groups, excitation of the MMCT transition led to the reduction of CO_2 gas loaded into the mesopores to CO by a single photon process under concurrent oxidation of Cu^{I} to Cu^{II}.[2] Also in the pores of MCM-41, water oxidation to O_2 was demonstrated by driving an Ir oxide nanocluster catalyst by an O-Cr^{VI} ligand-to-metal charge-transfer (LMCT) pump under visible light.[3]

In order to couple the H_2O oxidation and the CO_2 half reactions and thereby close the photosynthetic cycle, the next step is to replace the O-Cr^{VI} LMCT chromophore by a binuclear MMCT electron pump. The reason is that the free choice of partner metals of heterobinuclear units affords precise tuning of the redox energetics, which is necessary in order to couple the two half reactions and minimize overpotentials while maximizing the

visible absorption properties of the charge transfer chromophore. Specifically, the redox potential of the donor center of the MMCT unit (i.e. the metal center pulling electrons from the multi-electron transfer catalyst for water oxidation) needs to be in the range 1.3-1.8 V, which is dictated by the minimal potential for driving a multi-electron water oxidation catalyst (1.23 V)[4]. Donor metals like Cu^{I}, Sn^{II} used so far[1] do not have this property; these d^{10} and s^{2} metals were selected in our previous studies in order to facilitate the detection and identification of MMCT absorption of all-inorganic, binuclear units. For driving water oxidation catalysts, the first row transition metal Co^{III} is sufficiently oxidizing (E^{o} = 1.8 V)[5]. Therefore, photo-excitation of the charge-transfer unit Ti^{IV}-O-Co^{II} → Ti^{III}-O-Co^{III} would generate Co in an oxidation state that is energetically capable of driving a water oxidation catalyst.

In this paper, we report a synthetic procedure for the preparation of binuclear TiOCo sites on the surface of mesoporous silica MCM-41. Optical and FT-IR spectroscopy revealed a visible absorption tail of the MMCT unit and furnished evidence for covalent anchoring of the Co center.

2. Experimental Section

2.1 Synthesis of Materials

Siliceous MCM-41 sieve was prepared using previously described hydrothermal synthesis method,[1] except that the aging time in the autoclave at 110 °C was increased from previous 2 days to 3 days in order to assure complete silica condensation. The

grafting of Ti centers was conducted according to the titanocene dichloride method of Maschmeyer et al.[6], and standard Schlenk method was use throughout. Briefly, calcined MCM-41 powder (1.8 g) was dehydrated in a Schlenk tube at 250 °C under vacuum for 4 h. Titanocene dichloride (76.5 mg) was added under N_2 flow at RT. Following evacuation for 30 min, dichloromethane (80 mL) was vacuum distilled into the Schlenk tube. The suspension was stirred for 1h at RT to assure complete dissolution and diffusion of the $TiCp_2Cl_2$ into the silica mesopores. The base TEA (tetraethylamine, 0.8 mL) was added dropwise under nitrogen flow and the reaction continued under stirring for 5 h at RT. Over this period, the color of the suspension turned from red to pale yellow. The solution was filtered and the powder washed thoroughly with dichloromethane. The colorless filtrate confirmed that most of the $TiCp_2Cl_2$ was grafted onto MCM-41. Calcination of thus obtained pale yellow as-synthesized Ti-MCM-41 powder under flow of oxygen at 550 °C for 5h (preceded by ramp-up from RT to 550 °C over a period of 5 h) resulted in white, template free Ti-MCM-41 powder. Characterization by DRS, XANES and XRD confirmed grafting of Ti as isolated tetrahedral Ti centers. The Ti/Si ratio was 0.74 % per ICP analysis.

The bimetallic $TiCo^{II}$-MCM-41 was synthesized as follows. $CoCl_2$ (43.2 mg) was directly dissolved in acetonitrile (50 mL) in a Schlenk tube by stirring for 12 h at RT under nitrogen atmosphere (all subsequent operations were also conducted under N_2 flow). The solution was added to freshly calcined and dehydrated Ti-MCM-41 powder (1 g) in another Schlenk tube and stirred for 1h at RT, followed by addition of TEA (1 mL) and further stirring for 3 h at RT. The colorless supernatant indicated quantitative uptake

of Co^{II} into the silica pores. After filtration and washing with excess CH_3CN a pale blue powder was obtained. A typical Co/Ti ratio was 1.5 according to ICP analysis. For the synthesis of monometallic Co^{II}-MCM-41 (Co/Si = 1.5%), the same grafting procedure was used with calcined MCM-41 as starting material. Spectroscopic studies were conducted on $TiCo^{II}$ or Co^{II}-MCM-41 materials after heating at 350 °C under vacuum, or following calcination at 350 °C or 550 °C. The absence of significant changes in the XRD patterns of Co^{II}-MCM-41 and $TiCo^{II}$-MCM-41 compared to parent MCM-41 and Ti-MCM-41 indicated no loss of long-range ordering upon Ti and Co grafting (Supporting Information, Figure S2).[7,8]

For the preparation of a bimetallic sieve in which the Ti and Co are kept isolated, the as-synthesized Ti-MCM-41 sieve with the capping cyclopentadienyl ligand still attached to the grafted Ti centers was used. As a result, it is expected that subsequent anchoring of Co^{II} according to the method described above would not result in significant attachment of Co^{II} at Ti sites, but mainly to the surface silanol groups as in Co^{II}-MCM-41. For the synthesis of this material, the as-synthesized Ti-MCM-41 powder was dehydrated under vacuum at 150 °C and the other procedures are the same as described above for the synthesis of $TiCo^{II}$-MCM-41. Removal of the cyclopentadienyl from the final Ti-Co^{II}-MCM-41 product was accomplished by calcination at 350 °C or 550 °C. XRD measurements confirmed retention of the mesoporous long range ordering (Figure S2).[7] A typical Co/Ti ratio of the material was 1.2 according to ICP analysis.

The species formed upon dissolving $CoCl_2$ in acetonitrile is believed to be the tetrahedral complex $Co^{II}(NCCH_3)_2Cl_2$.[9] Therefore, this is very likely the species that reacts with the SiOH or TiOH groups on the pore surface. In order to test this assumption, $Co^{II}(NCCH_3)_2\,Cl_2$ was prepared according to literature procedure.[9] Cobalt dichloride (50 mg) was dissolved in acetonitrile (50 mL) in a Schlenk tube as described above. Removal of the solvent by evacuation at RT and recrystallization of the solid product in diethyl ether/acetonitrile (4:1) solution gave a blue powder. UV-visible spectrum (Co^{II} (d-d) peaks at 571, 614, 690 nm) and IR spectrum (Nujol, CH_3CN ligand absorptions at 2312, 2285 cm^{-1}) agreed well with the literature data.[7,9] The Co^{II}-MCM-41 was also synthesized using this isolated $Co^{II}(NCCH_3)_2Cl_2$ complex as cobalt precursor following the same procedure as described above. The optical and infrared spectra of the resulting material were the same as those of Co^{II}-MCM-41 prepared by directly dissolving $CoCl_2$ in CH_3CN, consistent with $Co(NCCH_3)_2Cl_2$ being the species that reacts with the silica surface.

Chemicals: cetyltrimethyl ammonium bromide, ammonium hydroxide (30%), tetraethyl orthosilicate, bis(cyclopentadienyl) titanium dichloride (titanocene dichloride, $TiCp_2Cl_2$), cobalt dichloride (anhydrous), Co(II) oxide, Co(II) hydroxide, Co(II,III) oxide (Co_3O_4), pyridine (anhydrous) were obtained from Aldrich and used as received. Diethyl ether was distilled over sodium and benzophenone; acetonitrile was distilled over CaH_2; dichloromethane was dried over 4Å molecular sieve activated at 400 °C; triethylamine (TEA) was dried over sodium. Ammonia (anhydrous) was obtained form Matheson Gas Inc.

2.2 Spectroscopy and Characterization

Optical spectra were measured on a Shimadzu model UV-2100 spectrometer equipped with an integrating sphere model ISR260. For measurement of mesoporous silica samples, the powder was pressed into a self-sustaining pellet and mounted in a home-built vacuum cell for diffuse reflectance measurements.[10] Barium sulfate was used as reference.

FT-IR spectra were recorded on a Bruker model IFS66V spectrometer equipped with LN_2 cooled MCT detectors Kolmar model KMPV8-1-J2 (8 μ bandgap), Infrared Associates (25 μ bandgap), or a DTGS detector (for 600-400 cm^{-1} region). Pressed self-sustaining pellets of mesoporous silica powder (5 mg) were mounted in a transmission infrared vacuum cell equipped with KBr windows. The loading of the infrared cell was done under N_2 atmosphere.

X-ray absorption near-edge structure (XANES) spectra of Ti-K edge were recorded at beamline 9.3.1 at the Advanced Light Source. The beamline is equipped with a Si(111) double-crystal scanning monochromator and operated at 1.9 GeV with beam current in the range of 200-400 mA. Measurements were conducted in the fluorescence mode using a Si photodiode detector (Hamamatsu S2744-08). The samples (ca. 20mg and 12 mm diameter) in the form of self-supporting wafers were evacuated at RT at 2×10^{-7} Torr for 2 h prior to the measurements. The Ti K-edge spectra were recorded at RT with sampling intervals of 0.2 eV and recording time of 2 sec per data point.

The powder XRD measurements were performed on a Siemens model D500 diffractometer equipped with Ni-filtered Cu-K_α radiation source (λ = 1.5406 Å). An accelerating voltage of 40 kV and a current of 30 mA were used for the X-ray setup. The textural uniformity of the MCM-41 materials was recorded for 2θ value over the range from

1.5° to 8° with a step size of 0.02° and a scanning rate of 1°/min. The XRD patterns of cobalt hydroxide, cobalt oxides, as well as the Co^{II}-MCM-41, $TiCo^{II}$-MCM-41 and Ti-Co^{II}-MCM-41 samples were also recorded over the range of 20° to 80° with a step size of 0.2° and scanning rate of 5°/min to probe for the presence of crystalline Co oxide clusters.

3. Results and Discussion

3.1 Single Co^{II} Centers Anchored in MCM-41

Established post-synthesis loading methods of Co^{II} onto mesoporous silica result in extensive formation of Co oxide clusters, particularly when using aqueous solutions of the Co precursor.[11,12] In order to achieve anchoring of isolated Co^{II} centers while minimizing the formation of Co oxide clusters, we have explored a Co^{II} grafting method using nonaqueous solutions of Co^{II} complexes featuring labile acetonitrile ligands. $Co^{II}(NCCH_3)_2Cl_2$ in acetonitrile was exposed to calcined, dehydrated MCM-41 powders under rigorous exclusion of moisture. Grafting was accelerated by addition of TEA (at 2% concentration) in order to activate the surface silanol groups. Figure 1, trace (a) shows the diffuse reflectance spectrum of the resulting Co^{II}-MCM-41 powder following evacuation at RT. The visible absorption with maxima at 545, 610, and 673 nm is characteristic of ligand field transitions ($^4A_2(F) \rightarrow {}^4T_1(P)$) of tetrahedral Co^{II},[13] and is very different from the d-d spectrum of octahedral Co^{II}.[14] Spectra of octahedral and tetrahedral Co^{II} in aqueous and acetonitrile solution, respectively are given in Figure S1 of the Supporting Information.[7] FT-IR spectra of as-synthesized Co^{II}-MCM-41 material after evacuation are presented in Figure 2, trace a, and show bands at 2987, 2954, 2889,

1477, 1460, 1394, and 733 cm^{-1}. The spectrum agrees well with that of TEA loaded into MCM-41. The sharp peak at 3745 cm^{-1} is due to free SiOH groups on the mesopore surface, while the broad absorption at 3400 cm^{-1} is due to residual traces of water. No physisorbed acetonitrile[1] or residual CH_3CN ligands bound to Co^{II} were observed. The latter have intense, characteristic C≡N stretch absorption at 2312 and 2285 cm^{-1} when coordinated to Co^{II}.[9] Absence of these bands indicates that no unreacted precursor remains in the silica pores, and that acetonitrile ligands are displaced completely upon grafting of the Co^{II} precursor onto the silica pore surface at room temperature, presumably by forming Co-O-Si linkages or coordination of Co^{II} to siloxane oxygen.

Removal of the residual TEA (and HCl) was accomplished by calcination in air or under oxygen gas flow. As can be seen from Figure 2, trace b, the corresponding infrared bands completely disappear when calcining the as-synthesized material for 5 h at 350 °C. No new absorptions are detected in the region 4000-500 cm^{-1}. Comparison of the noise level of the infrared spectrum for the Co^{II}-MCM-41 sample calcined at 350 °C with the intensity of the 669 and 583 cm^{-1} peaks of the mechanical mixture Co_3O_4/MCM-41 allowed us to conclude that at most 10 percent of the Co present in Co^{II}-MCM-41 is engaged in Co_3O_4 cluster formation. The more sensitive DRS spectrum of Co^{II}-MCM-41 calcined at 350 °C reveals the presence of small amount of Co_3O_4 clusters by a shoulder at 760 nm (Figure 1, trace b). From the height of the shoulder, we estimate that about 14 percent of the Co present in Co^{II}-MCM-41 is converted to Co_3O_4 clusters. No formation of clusters is observed when heating to 350 °C in vacuum; however, traces of TEA were found to remain in the pores under these conditions. Calcination at the substantially higher temperature of 550 ^oC did result in growth of infrared bands at 669 and 583 cm^{-1}

(Figure 2, trace c). They coincide with those of authentic spectra of Co_3O_4 mechanically mixed with MCM-41 particles (Figure S3)[7] and literature data.[15,16] The Co_3O_4 cluster formation upon calcination at 550 ^oC could also be observed in the XRD spectra (see Figure S2B (2θ = 31.2, 36.7, 59.4, 65.2^o).[7,11]

Grafted Co^{II} centers prepared by the method described above proved stable in aqueous solution. After repeated washing with water, a small blue shift of the visible ligand field peaks by 10-15 nm was observed, but no significant loss of intensity or change from tetrahedral coordination was noted (Figure 1, trace c).

From inspection of the 1000-500 cm^{-1} infrared region of Co-MCM-41, it is not obvious whether modes associated with Co-O-Si linkages absorb in this region. Detection of these modes tends to be challenging because the corresponding bands are typically tens of cm^{-1} wide and may overlap with silica lattice absorptions; the asymmetric SiO_2 stretch extends from 1270 – 970 cm^{-1}, the symmetric SiO_2 stretch from 820 - 780 cm^{-1}. Nevertheless, we have found recently that metal-oxygen bond modes can be identified by action spectroscopy.[1,2] In the case of Co-MCM-41, exposure of the sieve to NH_3 gas resulted in changes of the Co^{II} coordination that revealed bands associated with Co-O-Si linkages. Figure 3a shows the difference spectrum of Co-MCM-41 after (minus before) exposure of the pellet to 3 Torr NH_3 and subsequent evacuation for 1 h at RT. Absorbance growth at 3365, 3287, 3222, and 3194 cm^{-1} is attributed to NH stretch vibrations, while bands at 1619 and 1452 cm^{-1} are in a region where NH bending modes absorb.[17] More specifically, the strong peaks at 3365, 3287 and 1619 cm^{-1} are very close to the asymmetric and symmetric stretch and bending modes of ammine ligands of Ni^{II}

centers grafted onto MCM-41.[18] Therefore, we assign the 3 bands to NH_3 coordinated to Co^{II} anchored on the pore surface. The weak absorptions at 3222, 3194, and 1452 cm^{-1} are commonly associated with NH_4^+.[19-22] The formation of Co-NH_3 ligands is accompanied by absorbance loss at 831 and 762 cm^{-1} as can been seen from Figure 3, trace a. No such negative features were observed when exposing ammonia to neat MCM-41. We propose assignment of the 831 and 762 cm^{-1} bands to Co-O modes of Co-O-Si linkages that are replaced by Co-NH_3 bonds upon loading of NH_3 gas. The absorptions, which are in the same spectral region where the symmetric CoO stretching mode of CoO_4 tetrahedra absorb (790 cm^{-1}),[23] furnish evidence for covalent anchoring of the Co centers on the silica pore surface.

3.2 Binuclear TiOCo Sites in MCM-41

Binuclear $TiOCo^{II}$ sites were assembled by loading the $Co(NCCH_3)_2Cl_2$ precursor into calcined Ti-MCM-41 sieve as described in the Sect. 2. We anticipate preferential reaction of the precursor with TiOH groups because of the higher acidity of titanol compared to silanol groups as indicated by a red shift of the OH stretch mode.[24,25] This may result in a higher proportion of bimetallic sites relative to isolated Co^{II} centers than predicted by the relative abundance of TiOH and SiOH groups. Infrared spectra of the as-synthesized sample did not exhibit any residual CH_3CN ligands. As in the case of Co-MCM-41, heating under oxygen flow at 350 ^oC removed TEA completely (Figure 2, trace d). Comparison of the $TiCo^{II}$-MCM-41 infrared spectrum with that of Co^{II}-MCM-41 (Figure 2, trace b) shows a 10 cm^{-1} red shift of the 975 cm^{-1} silica band upon Ti

anchoring, and a shoulder at 945 cm^{-1} that is not present in the monometallic Co material. Both bands are attributed to Si-O stretch vibrations of silica moieties perturbed by the presence of Ti centers.[1,26-28] The NH_3 action difference spectrum, trace b of Figure 3, shows depletion at 830 and 760 cm^{-1} assigned to Co-O modes of anchored Co centers (the peaks of the two depletion bands varied by a few cm^{-1} from sample to sample, which prevented us from discerning small shifts due to the presence of Ti). These depletions were absent when conducting the NH_3 adsorption experiment with (Co-free) Ti-MCM-41, as can be seen from Figure 3, trace d. In this case, only weak bands due to NH_3 coordinated to Ti (3399, 3292, 1608 cm^{-1}) and ammonium ions (1658, 1452 cm^{-1}) were observed, in agreement with literature.[29] No Co oxide clusters were detected for this bimetallic material in the infrared even upon calcination at 550 ^oC.

Figure 4 shows UV-Visible diffuse reflectance spectra of the resulting $TiCo^{II}$-MCM-41 materials after heating under vacuum at 350 ^oC (panel A) or upon calcination at 550 ^oC (panel B). In each case, the spectrum of the correspondingly treated Co^{II}-MCM-41 sample and the superposition of the Ti-MCM-41 and Co^{II}-MCM-41 spectra are shown for comparison (the Ti-MCM-41 spectrum has no optical absorption at λ>330 nm). The $TiCo^{II}$-MCM-41 sieve exhibits a continuous absorption tail extending from the UV to around 600 nm in the red that is not present in the monometallic Co material. We attribute the new absorption to the $Ti^{IV}/Co^{II} \rightarrow Ti^{III}/Co^{III}$ MMCT transition. The relative intensity change of the peaks of the Co^{II}(d-d) absorption profile upon treatment at 550^oC compared to 350^oC is typical for high temperature treatment of sieves containing tetrahedral Co^{II} centers.[30] While no Co_3O_4 cluster formation was detected by DRS for $TiCo^{II}$-MCM-41 subjected to heating at 350 ^oC under vacuum (Figure 4A), a shoulder is

observed at 760 nm for $TiCo^{II}$-MCM-41 calcined at 550 ^{o}C (Figure 4B). However, the band is much smaller than for the monometallic Co^{II}-MCM-41 sieve, in agreement with the much lower yield of Co_3O_4 measured by XRD, shown in Figure S2B.

The assignment of the new UV-Visible absorption band to a $Ti^{IV}/Co^{II} \rightarrow Ti^{III}/Co^{III}$ charge transfer transition is further supported by comparison of the TiCo-MCM-41 sample with an MCM-41 sieve containing Ti and Co centers that are deliberately kept separated. The material, denoted Ti-Co^{II}-MCM-41, was prepared by exploiting the cyclopentadienyl capping ligand as a protective group against substitution of Co at the Ti center according to the procedure described in Sect. 2. As can be seen from Figure 5, the DRS of Ti-Co^{II}-MCM-41, trace a, is almost the same as a superposition of the spectra of monometallic Ti-MCM-41 and Co^{II}-MCM-41 (Figure 5, trace c) and does not show the continuous absorption tail of $TiCo^{II}$-MCM-41 (Figure 5b). Yet, the presence of grafted Ti and Co centers in Ti-Co^{II}-MCM-41 is clearly demonstrated by the Co-O-Si and Ti-O-Si bond modes detected in the infrared at 762, 831 and 934 cm^{-1} (Figure 3, trace c). Absorbance loss of Ti-perturbed silica modes at 934 cm^{-1}, but not at 965 cm^{-1}, suggests that only Ti sites that give rise to the 934 cm^{-1} band interact with ammonia. Clearly, the appearance of the MMCT absorption band requires a linkage between Ti and Co centers. The substitution reaction of the $Co(NCCH_3)_2Cl_2$ at the TiOH center that results in the formation of the MMCT absorption suggests that the two metal centers are linked by an oxo bridge. Therefore, we assign the UV-Visible absorption tail to a Ti^{IV}-O-$Co^{II} \rightarrow Ti^{III}$-O-$Co^{III}$ charge-transfer transition and conclude that the $TiCo^{II}$-MCM-41 sieve has anchored TiOCo units along with isolated Co and Ti sites.

In order to investigate the possibility of a hydroxo rather than an oxo bridge between the anchored Ti and Co centers, a $TiCo^{II}$-MCM-41 material calcined at 350 ^{o}C was exposed to 3 Torr pyridine gas. Pyridine is known to convert quantitatively to pyridinium upon exposure to Bronsted acid sites such as bridging hydroxyl groups, giving rise to a characteristic infrared band at 1545 cm^{-1}.[31] As can be seen from the FT-IR difference spectrum of Figure 6, trace b, no pyridinium is observed, just pyridine interacting with Co^{II}. The latter acts as weak Lewis acid, giving rise to an absorption band at 1450 cm^{-1}. We conclude that there is no evidence for the presence of Ti-O(H)-Co linkages.

Comparison of Ti K-edge XANES spectra of $TiCo^{II}$-MCM-41, Co^{II}-MCM-41, and Ti-Co^{II}-MCM-41 materials furnish additional evidence for a change of the coordination geometry in the case of the $TiCo^{II}$ units. Figure 7A shows the K-edge absorption spectra of the three samples, and Figure 7B the Ti A_1-T_2 pre-edge peak on an expanded scale (the peak at 4968 eV is taken as the origin of the energy scale). As previously observed for the case of $TiCu^{I}$-MCM-41[1] and reported earlier as evidence for the distortion of tetrahedrally coordinated Ti,[32] the intensity decrease and small but reproducible blue shift of 0.2 eV of the pre-edge peak is consistent with distortion of the Ti coordination from tetrahedral geometry due to formation of an oxo bridge to another metal center.

There are precedents for Ti-O-Co^{II} moieties in other solid environments. Eldewick and Howe[23] have reported oxo-linked Ti-O-Co^{II} centers in microporous titanosilica material of type ETS-10. The structure of ETS-10 comprises corner-sharing

SiO_4 tetrahedra and TiO_6 octahedra linked through bridging oxygens.[33] In the bimetallic Co-ETS-10 sieve, the cobalt centers were found to isomorphically substitute Si sites adjacent to TiO_6 octahedra based on EXAFS evidence.[23] A visible absorption tail extending beyond 500 nm is observed, which is not present in monometallic ETS-10. Metal-to-metal charge-transfer $Ti^{IV}OCo^{II} \rightarrow Ti^{III}OCo^{III}$ is the only conceivable assignment for the new absorption band. Furthermore, the color of many dense phase, mixed metal oxides have long been attributed to MMCT transitions. Specifically, Co^{II}-doped titanate $MgTi_2O_5:Co^{II}$ exhibits a strong continuous $Ti^{IV}OCo^{II} \rightarrow Ti^{III}OCo^{III}$ absorption tail extending from the UV region to about 700 nm. The band is overlapped by, but clearly distinguishable from the Co^{II} ligand field transitions.[34,35]

According to a theory first laid out by Hush, aside from the reorganization energy, the MMCT transition energy depends on the ionization energy of the divalent donor and the electron affinity of the acceptor metal center.[36] As a consequence, other divalent transition metal ions oxo-bridged to Ti^{IV} are likely to give rise to MMCT transitions absorbing in the visible as well because their ionization potentials are relatively close to each other.[37] In fact, a number of divalent first row transition metal titanates absorb in the visible.[34,35,38] The monotonous increase of the onset of the MMCT absorption band for Fe^{II}, Mn^{II}, Co^{II}, and Ni^{II} titanates from the near infrared to the green spectral region reflects the ordering of the ionization potentials of the metal centers.[34] These observations on solid mixed metal oxides indicate that assembly of corresponding binuclear $TiOM^{II}$ moieties on silica mesopore surfaces may open up access to visible light-absorbing redox sites with tunable oxidation properties.

4. Conclusions

In summary, a grafting method in non-aqueous media is reported that affords anchoring of single Co centers on the surface of silica mesopores in the absence of significant Co oxide cluster formation. The formation of binuclear Ti-O-Co units is evidenced by the observation of a Ti^{IV}-O-Co^{II} → Ti^{III}-O-Co^{III} charge-transfer chromophore extending throughout the visible to 600 nm, and infrared bands assigned to Co-O-Si linkages. A more detailed study of the coordination environment of each metal and the geometry of the oxo bridge by EXAFS is planned.

The $TiCo^{II}$-MCM-41 material reported here expands the range of mesoporous silicas featuring visible light absorbing MMCT units anchored on the pore surface in terms of coverage of the visible spectrum and accessible redox potentials. In particular, Co^{III} generated upon MMCT excitation of the Ti-O-Co^{II} site is energetically capable of driving a multi-electron transfer catalyst for H_2O oxidation.

Acknowledgment

This work was supported by the Director, Office of Science, Office of Basic Energy Sciences, Division of Chemical, Geological and Biosciences of the U.S. Department of Energy under Contract No. DE-AC03-76SF00098.

References

1. W. Lin, H. Frei, J. Phys. Chem. B 109 (2005) 4929.

2. W. Lin, H. Frei, J. Am. Chem. Soc. 127 (2005) 1610.

3. R. Nakamura, H. Frei, J. Am. Chem. Soc. 128 (2006) 10668.

4. J.P. Hoare, in: A.J. Bard, R. Parson, J. Jordan (Eds.), Standard Potentials in Aqueous Solution, Marcel Dekker, New York, 1985, p. 65.

5. N. Maki, N. Tanaka, in: A.J. Bard, R. Parson, J. Jordan (Eds.), Standard Potentials in Aqueous Solution, Marcel Dekker, New York, 1985, p. 381.

6. T. Maschmeyer, F. Rey, G. Sankar, J.M. Thomas, Nature 378 (1995) 159.

7. Supporting Information

8. J.S. Beck, J.C. Vartuli, W.J. Roth, M.E. Leonowicz, C.T. Kresge, K.D. Schmitt, C.T.W. Chu, D.H. Olson, E.W. Sheppard, S.B. McCullen, J.B. Higgins, J.L. Schlenker, J. Am. Chem. Soc. 114 (1992) 10834.

9. B.J. Hathaway, D.G. Holah, J. Chem. Soc. (1964) 2400.

10. F. Blatter, F. Moreau, H. Frei, J. Phys. Chem. 98 (1994) 13403.

11. J. Panpranot, S. Kaewkun, P. Praserthdam, J.L. Goodwin, Catal. Lett. 91 (2003) 95.

12. Q. Tang, Q. Zhang, H. Wu, Y. Wang, J. Catal. 230 (2005) 384.

13. A.B.P. Lever, Inorganic Electronic Spectroscopy, 2nd Ed., Elsevier, Amsterdam, 1984, p. 496.

14. A.B.P. Lever, Inorganic Electronic Spectroscopy, 2nd Ed., Elsevier, Amsterdam, 1984, p. 480.

15. S. Lim, D. Ciuparu, Y. Chen, L. Pfefferle, G.L. Haller, J. Phys. Chem. B 108 (2004) 20095.

16. G. Busca, R. Guidetti, V. Lorenzelli, J. Chem. Soc. Farad. Trans. 86 (1990) 989.

17. K. Schmidt, W. Hauswirth, A. Muller, J. Chem. Soc., Dalton Trans. (1975) 2199.

18. D. Bruhwiler, H. Frei, J. Phys. Chem. B 107 (2003) 8547.

19. J.M. Fletcher, B.F. Greenfield, C.J. Hardy, D. Scargill, J.L. Woodhead, J. Chem. Soc. (1961) 2000.

20. M.R. Basila, T.R. Kantner, J. Phys. Chem. 71 (1967) 467.

21. K. Brodersen, H.J. Becher, Chem. Ber. 89 (1956) 1487.

22. K. Niwa, H. Takahashi, K. Higasi, T. Kajiura, Bull. Chem. Soc. Jpn. 44 (1971) 3010.

23. A. Eldewik, R.F. Howe, Microporous Mesoporous Mater. 48 (2001) 65.

24. W. Lin, H. Frei, J. Am. Chem. Soc. 124 (2002) 9292.

25. M.S. Morey, S. O'Brien, S. Schwarz, G.D. Stucky, *Chem. Mater.* 12 (2000) 898.

26. W.S. Ahn, D.H. Lee, T.J. Kim, J.H. Kim, G. Seo, R. Ryoo, Appl. Catal. A: General 181 (1999) 39.

27. M.E. Raimondi, E. Gianotti, L. Marchese, G. Martra, T. Maschmeyer, J.M. Seddon, S. Coluccia, J. Phys. Chem. B 104 (2000) 7102.

28. M.S. Morey, J.D. Bryan, S. Schwarz, G.D. Stucky, Chem. Mater. 12 (2000) 3435.

29. Y. Hu, G. Martra, J. Zhang, S. Higashimoto, S. Coluccia, M. Anpo, J. Phys. Chem. B 110 (2006) 1680.

30. K. Nakashiro, Y. Ono, Bull. Chem. Soc. Jpn. 66 (1993) 9.

31. B. Kraushaar, W.G.M. Hoogervorst, R.R. Andrea, C.A. Emeis, W.H.J. Stork, J. Chem. Soc. Faraday. Trans. 87 (1991) 891.

32. G. Sankar, J.M. Thomas, C.R.A. Catlow, C.M. Barker, D. Gleeson, N. Kaltsoyannis, J. Phys. Chem. B 105 (2001) 9028.

33. M.W. Andersen, O. Terasaki, T. Ohsuna, T.; A. Philippou, S.P. MacKay, A. Ferreira, J. Rocha, S. Lidin, Nature 367 (1994) 347.

34. G. Blasse, G.J. Dirksen, Chem. Phys. Lett. 77 (1981) 9.

35. G. Blasse, Structure and Bonding 76 (1991) 153.

36. N.S. Hush, Prog. Inorg. Chem. 8 (1967) 391.

37. D.R. Lide, CRC Handbook of Chemistry and Physics, 85th Ed., CRC Press, Boca Raton, 2004, p. 10-183.

38. G. Blasse, P.H.M. De Korte, A. Mackor, J. Inorg. Nucl. Chem. 43 (1981) 1499.

Figure Captions:

Fig 1: DRS spectra of Co^{II}-MCM-41: a) as-synthesized; b) calcined at 350 °C in air; c) after washing the as-synthesized sample with H_2O. For comparison, the spectra were normalized according to the highest Co^{II} d-d band at 650-670 nm.

Fig 2: FTIR spectra of Co-MCM-41: a) as-synthesized; b) calcined in air at 350 °C; c) calcined in air at 550 °C. d) TiCo-MCM-41 calcined at 350 °C in air. The broad band at 1650 cm^{-1} is due to overlapping silica combination and residual water absorption.

Fig 3: FTIR difference spectra of NH_3 adsorption (3 Torr, followed by 1 h evacuation) on a) Co^{II}-MCM-41; b) $TiCo^{II}$-MCM-41; c) Ti-Co^{II}-MCM-41; and d) Ti-MCM-41. Prior to NH_3 adsorption at room temperature, cobalt containing samples were calcined at 350 °C and Ti-MCM-41 at 550 °C in air.

Fig 4: DRS spectra of A: 1) $TiCo^{II}$-MCM-41; and 2) Co^{II}-MCM-41, and 3) addition of the spectra of 2) Co^{II}-MCM-41 and of calcined Ti-MCM-41. Both samples were heated at 350 °C under vacuum. B: 1) $TiCo^{II}$-MCM-41; 2) Co^{II}-MCM-41; and 3) addition of the spectra of 2) Co^{II}-MCM-41 and of calcined Ti-MCM-41. Both samples were calcined at 550 °C in air.

Fig 5: DRS spectra of calcined (550 °C) a) Ti-Co^{II}-MCM-41and b) $TiCo^{II}$-MCM-41; and c) addition spectrum of Ti-MCM-41 and Co^{II}-MCM-41.

Fig 6: FTIR difference spectra of pyridine adsorption experiments on a) Co^{II}-MCM-41 and b) $TiCo^{II}$-MCM-41. Both samples were calcined in air at 350 °C.

Fig.7: XANES spectra of A: a) Ti-MCM-41; b) Ti-Co-MCM-41; c) TiCo-MCM-41. All samples were calcined at 350 ^{o}C in air. The absorption intensity was normalized for the total amount of Ti as measured by the height of the plateau between the K-edge and the onset of the EXAFS region. B: Pre-edge peaks of the 3 samples on expanded scale. The A_1-T_2 pre-edge peak at 4968 eV is taken as the origin of the energy scale.

Fig 1:

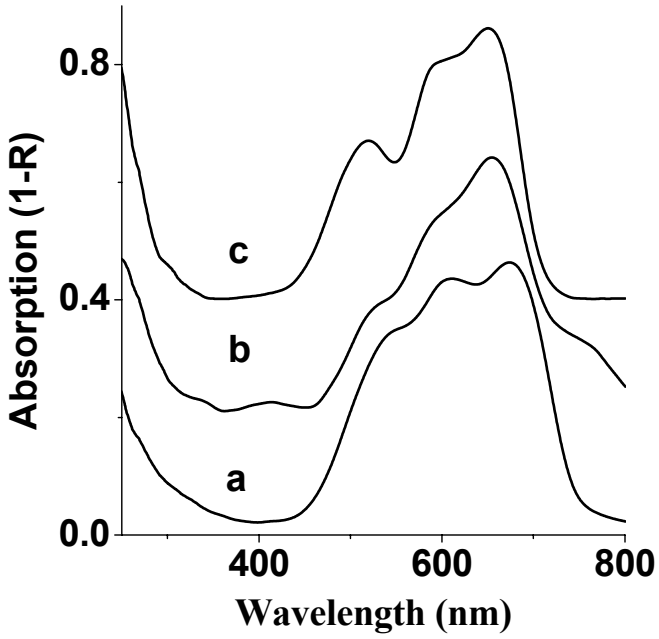
Absorption (1-R)
0.8
0.4
0.0
400
600
800
Wavelength (nm)
a
b
c

Fig 2:

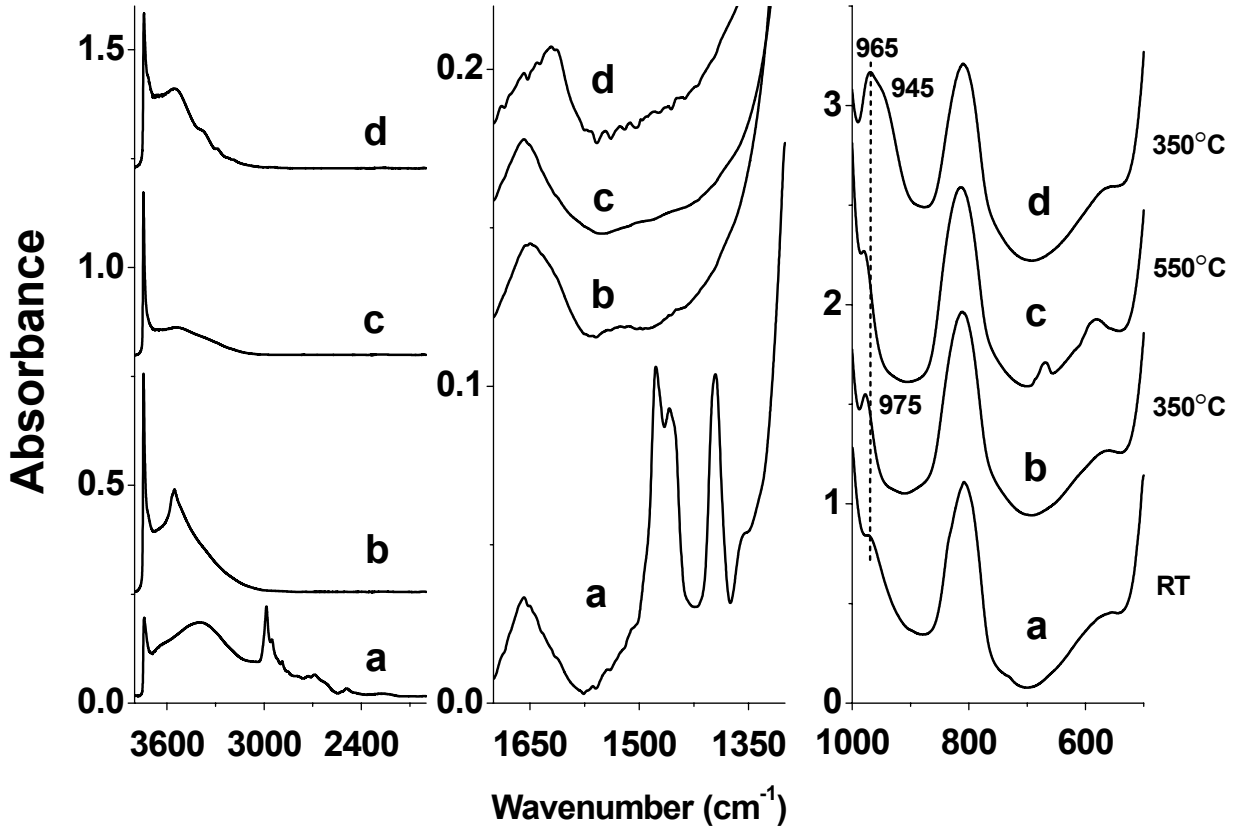
Absorbance
1.5
1.0
0.5
0.0
3600
3000
2400
d
c
b
a
0.2
0.1
0.0
1650
1500
1350
965
945
975
3
2
1
0
1000
800
600
350°C
550°C
350°C
RT
Wavenumber (cm-1)

Fig 3:

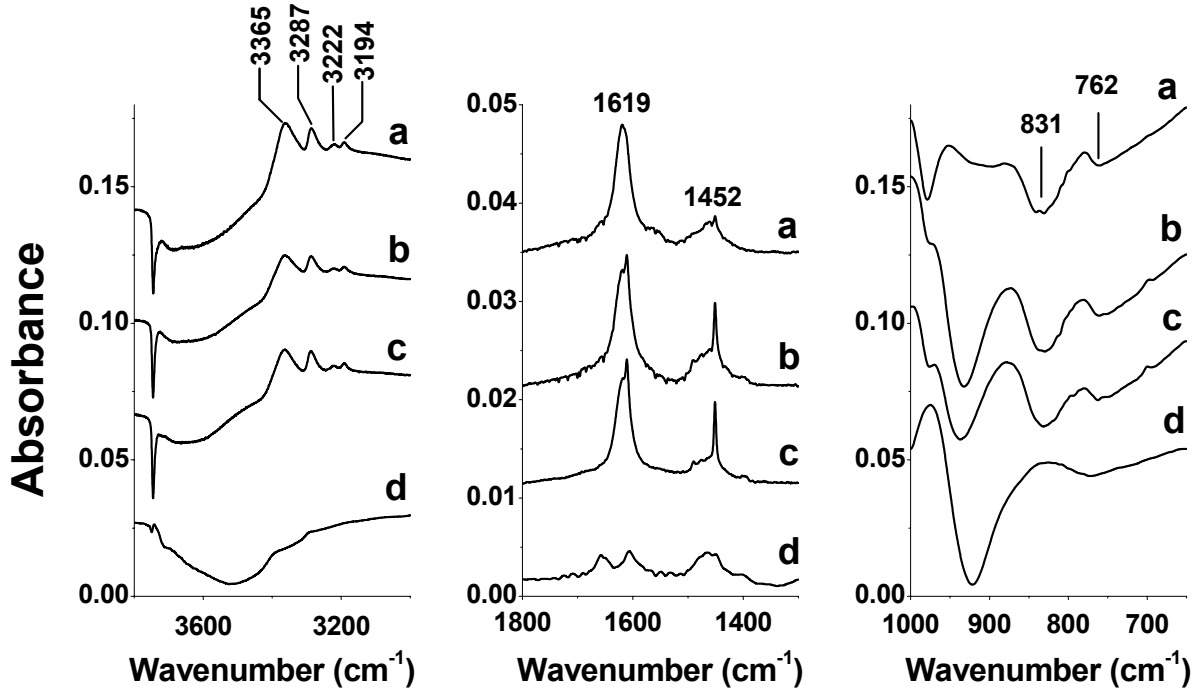
3365
3287
3222
3194
a
b
c
d
Absorbance
0.15
0.10
0.05
0.00
3600
3200
Wavenumber (cm-1)
1619
1452
0.05
0.04
0.03
0.02
0.01
0.00
1800
1600
1400
Wavenumber (cm-1)
762
831
1000
900
800
700
Wavenumber (cm-1)

Fig 4:

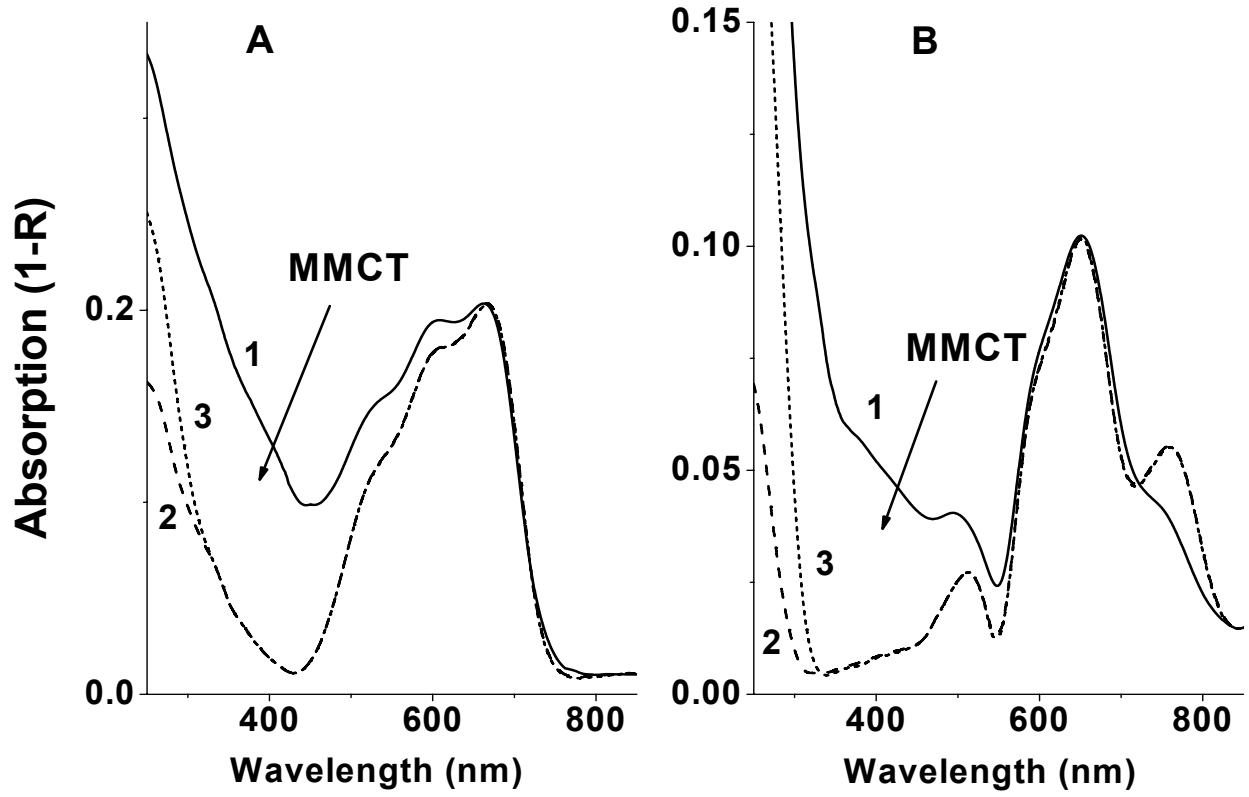
A
B
MMCT
1
2
3
Absorption (1-R)
0.2
0.0
0.15
0.10
0.05
0.00
400
600
800
Wavelength (nm)

Fig 5:

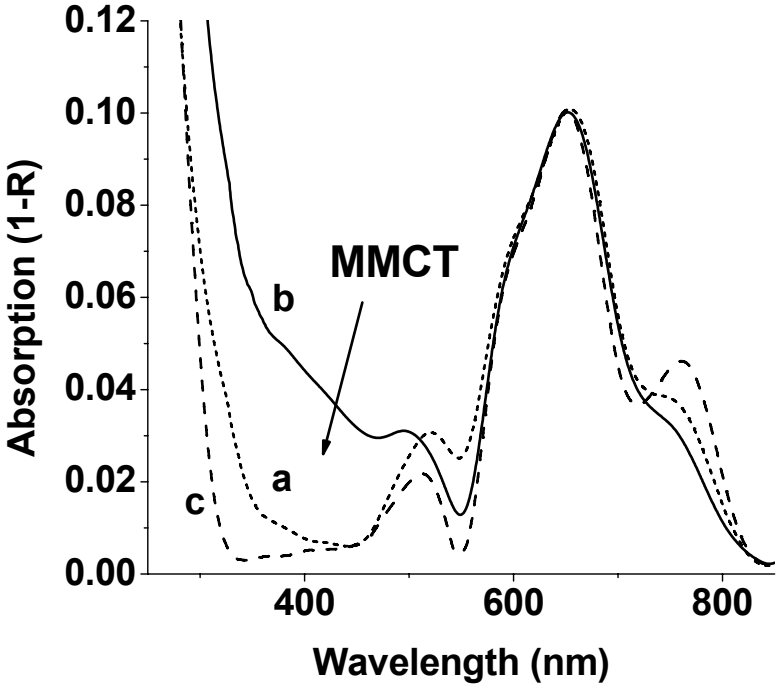
0.12
0.10
0.08
0.06
0.04
0.02
0.00
Absorption (1-R)
MMCT
b
a
c
400
600
800
Wavelength (nm)

Fig 6:

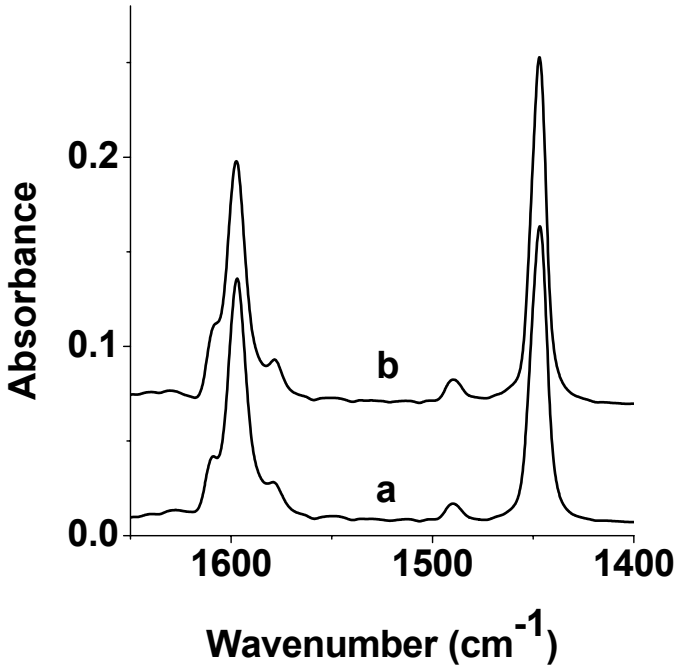
0.2
0.1
0.0
Absorbance
b
a
1600
1500
1400
Wavenumber (cm-1)

Fig 7:

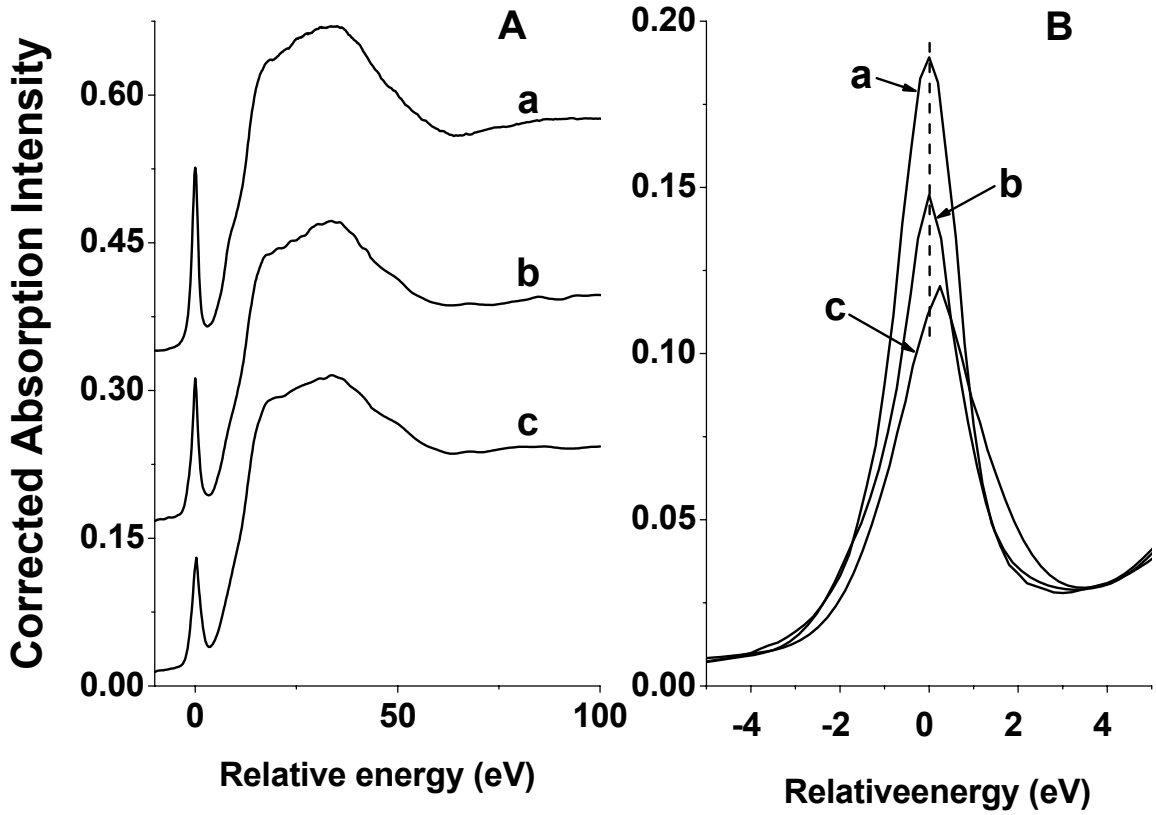
A
B
a
b
c
Corrected Absorption Intensity
0.00
0.15
0.30
0.45
0.60
0
50
100
Relative energy (eV)
0.00
0.05
0.10
0.15
0.20
-4
-2
0
2
4
Relativeenergy (eV)